16th World Conference on Earthquake, 16WCEE 2017

Santiago Chile, January 9th to 13th 2017

Paper N° 2771

Registration Code: S-F1464562996

LOCAL STRESS DROP ESTIMATES OF STRONG EARTHQUAKES IN THE SOUTH ICELAND SEISMIC ZONE

T. Sonnemann(1), B. Halldorsson(2), B. Hrafnkelsson(3), A. S. Papageorgiou(4)

(1) *Ph.D. Student, Earthquake Engineering Research Centre & Faculty of Civil and Environmental Engineering, School of Engineering & Natural Sciences, University of Iceland, Selfoss, Iceland, tsonne@hi.is*

(2) *Research Professor & Director of Research, Earthquake Engineering Research Centre. Faculty of Civil and Environmental Engineering, School of Engineering & Natural Sciences, University of Iceland, Selfoss, Iceland, skykkur@hi.is*

(3) *Professor, Faculty of Physical Sciences, School of Engineering & Natural Sciences, University of Iceland, birgirhr@hi.is*

(4) *Professor, Department of Civil Engineering, University of Patras, Rio-Patras, Greece, papaga@upatras.gr*

Abstract

In earthquake prone regions where strong-motion data is scarce, the reliability of strong ground motion simulations from large earthquakes depends heavily on realistic source, path and site models. Due to the inherent uncertainty and randomness of earthquake processes and crustal heterogeneities, reducing the standard error associated with empirical attenuation relationships has proven difficult. Additionally, such relationships are strictly speaking not valid outside the range that the data defines. Therefore, it is advantageous to use physically based models, especially of the earthquake source, for ground motion simulation. The specific barrier model (SBM) provides a complete, yet parsimonious and self-consistent description of the faulting processes that are responsible for the generation of high-frequency waves (> 1 Hz). It is especially versatile and has, when modeling the earthquake as a point-source, been applied in the context of the stochastic modeling approach and random vibration theory. Moreover, modeling the earthquake on a finite-size fault, the SBM has also been applied in more physically realistic strong-motion hybrid-simulations, both in the near-fault as well as far-field region of a finite earthquake source. While previous studies have successfully simulated key parameters of strong-motion and complete time histories, the uncertainty of the source parameters has not been quantified. A key source parameter of the SBM is the local stress drop which drives the slip on the fault. In this study, using the strong-motion database of Iceland, the most seismically active region in northern Europe, as a case-study, moderate-to-strong Icelandic earthquakes (77 records of 6 earthquakes in the South Iceland Seismic Zone with M_W ranging from 5.1 to 6.5) were modeled by the SBM and their local stress drops estimated. While the SBM provides a simple but physically meaningful representation of the faulting process the Bayesian method gives mathematically well-defined answers to the question what we can learn about the stress drop value distribution from the given data. Therefore, the model parameter uncertainty was quantified within the Bayesian statistical framework, employing a Markov chain Monte Carlo (MCMC) method with the Metropolis algorithm. To set up the Bayesian probability system, the data were corrected for path and site effects to obtain derived source spectra for each earthquake. In order to avoid trade-offs with the local stress drop, the high-frequency diminution parameter κ was determined independently using a new automated scheme developed in this study. The results show that the uncertainties of local stress drop are constant for the earthquakes analyzed, and are lognormally distributed. Median values of interevent local stress drops are consistent with the exception of one event, the far-field data of which are contaminated by ground motions from triggered earthquakes. The results for the earthquakes in the South Iceland Seismic Zone are the first step towards applying a physically consistent earthquake source and ground motion model in strong-motion simulations from earthquake scenarios in North Iceland where the lack of data preclude such calibrations.

Keywords: local stress drop, specific barrier model, Bayesian statistics

1. Introduction

Earthquake strong-motion simulation for earthquake engineering applications is of primary importance for the estimation of earthquake hazard and with direct implications for seismic risk assessment. Such simulations are generally based on seismological models that have been calibrated on the basis of recorded data for the region under study. While earthquake strong-motion records show considerable variability in key parameters such as peak ground acceleration and derived quantities such as spectral response, for a given earthquake magnitude and distance this variability is generally not captured, especially by empirical ground motion models. However, this variability is especially important in various practical applications such as fragility analyses. In order to effectively incorporate such variability into simulations without losing sight of the physical meaning of the origin of the variability, one should use a seismological model that is centered on a simple, yet physically realistic model of the earthquake source. The specific barrier model provides the most complete, yet parsimonious, self-consistent description of the earthquake faulting process and applies both in the near-fault and far-field region [1–4]. The seismic moment is distributed on the fault plane via subevents on the basis of moment and area constraints. Thus, the model allows for consistent ground motion simulations over a large range of frequencies and distances. For simulations in the far-field region the source acceleration spectrum exists in analytical form and accounts for a high degree of earthquake source complexity and source-site geometry [5–7]. In the near-fault region, the near-fault velocity pulses, which are the most characteristic feature of near-fault strong-motion, scale with key parameters of the specific barrier model and may effectively be simulated using a phenomenological model [8,9]. The key parameter of the SBM is the local stress drop $\Delta\sigma_L$ which controls the high-frequency level of radiated seismic waves. For the application of the model for engineering purposes the local stress drop needs to be determined for the region under study. Moreover, its variability, both interevent and intraevent needs to be evaluated so that the variation of the source radiation can be accounted for in the simulation. Morover, the variation provides insight into the level of source complexity of the earthquakes studied, which may guide in the application of the model for near-fault simulations [7].

This study therefore deals with the inference of the local stress drop within the Bayesian framework from spectral ground acceleration amplitude data while using the SBM to generate synthetic source acceleration spectra and employing a Markov chain Monte Carlo (MCMC) method with the Metropolis algorithm. The data used is from accelerometer measurements on the Icelandic strong-motion network of earthquake ground shaking originating from significant earthquakes that occurred from 1987 to 2008 in South Iceland. The local stress drop mainly influences the high frequency (>1 Hz) part of the Fourier amplitude source acceleration spectrum, which means that it partly trades off with a high frequency spectral decay generally theorized as Kappa (κ) filter. The origin of this decay has been attributed to site [10], site and path [11] and source effects [2], and there are various measurement methods of this parameter [12]. To better constrain the stress drop values, we measured κ values independently of the subsequent $\Delta\sigma_L$ inference as prior information. After testing the inference for the effects of various frequency spacings, site amplification assumptions as well as lower and upper frequency limits, a final parameter configuration was selected as optimal for the inversion. While the distributions of $\Delta\sigma_L$ for the six chosen earthquakes were obtained, the question remained as to how much influence the other seismological parameters would have. The uncertainty attributed to stress drop in this case contains the site and path variations as well and thus overestimates it. A different setup using pseudo-spectral accelerations was then employed with more free parameters and a random effects model comparable to that of Abrahamson and Youngs [13]. That way, co-dependent parameter distributions were better quantified, the parameters' uncertainties better represent the given data and the inferred estimates became much narrower.

2. Data

The input data are ground acceleration measurements generated by medium-sized earthquakes from 1987 to 2008 (*Table 1*). The seven earthquakes are all located in the South Iceland Seismic Zone (SISZ, see *Fig. 1*) and the magnitude range chosen is from M_W 5.1 to 6.5. The events were recorded by 5 to 24stations, and for each record the shear wave arrival time was determined manually. The accelerometric stations belong to the Icelandic strong-motion network (ISMN) of the Earthquake Engineering Research Centre of the University of Iceland [14]. While most stations are set up to directly measure ground response (i.e., free-field), some stations are parts of structural monitoring systems located within power stations, office buildings and in bridges. All instruments record acceleration on three orthogonal components, but only the horizontal ones were used for the analysis. Most stations' sampling frequencies are 200 Hz, but some record at 100 Hz. As the instruments measure ground movement, the immediate subsurface characteristics are relevant to the measurements. Most stations are located on what is generally referred to as rock, but some stations are located on stiff soil [15,16].

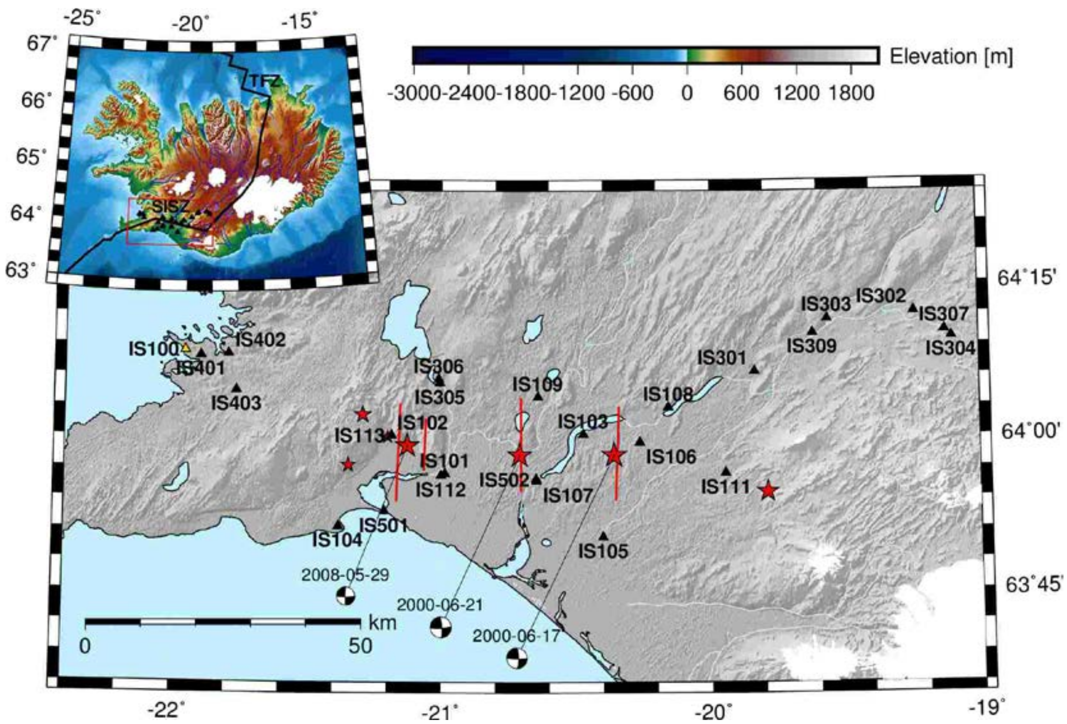

Fig. 1 – The left-hand inset shows the plate boundary across Iceland, the locations of the South Iceland Seismic Zone (SISZ) and the Tjörnes Fracture Zone (TFZ) as well as the study area indicated by a rectangle. All earthquakes and stations used in this study are located in or close to the SISZ. The stars indicate epicenters of the studied earthquakes, which are scaled to magnitude. For the three largest events, moment tensor solutions from the USGS and fault lines are shown as well. The labeled triangles represent accelerometer stations, of which only station IS100 has not been used in this study.

Table 1 - List of SISZ events used in this study. N_{rec} I and N_{rec} II refer to the number of records used in the inference method using FAS for stress drop only and using SA with the random effects model, respectively.

Ev.ID	YYYY-MM-DD	hh:mm:ss	latitude	longitude	M_W	N_{rec} I	N_{rec} II
1	1987-05-25	11:31:56.0	63.9100	-19.7900	6.0	6	7
2	1992-12-27	12:23:21.0	64.0000	-21.2000	4.8	0	5
3	1998-06-04	21:36:54.0	64.0360	-21.2930	5.4	11	11
4	1998-11-13	10:38:34.0	63.9540	-21.3460	5.1	8	8
5	2000-06-17	15:40:41.0	63.9700	-20.3600	6.5	20	17
6	2000-06-21	00:51:48.0	63.9700	-20.7100	6.4	24	23
7	2008-05-29	15:45:59.0	64.0110	-21.0063	6.3	8	8

3. Physical Theory

To adequately describe observed SGM data, a theoretical model is used whose parameters have partially been calibrated to earthquakes in the SISZ [17]. However, these values did not include uncertainty estimates, which are typically required in seismic hazard studies and other earthquake engineering applications to characterize observed variability[18]. As the near-surface attenuation parameter κ_r significantly influences the spectra at high frequencies where the model is most sensitive to changes in local stress drop $\Delta\sigma_L$, a significant trade-off between these parameters is expected. This could be avoided by first independently measuring κ_r, which would also account for the fact that $\Delta\sigma_L$ is source-dependent, whereas κ_r needs to be determined for each site individually regardless of the respective source.

3.1 Kappa measurement

Anderson and Hough [11] have defined a spectral decay parameter κ which reportedly quantifies near-surface anelastic attenuation and they proposed a way of measuring it from acceleration spectra. This parameter has been characterized in various ways owing to different interpretations as to its origin, and a general form was presented by Ktenidou et al. [12], resolving the traditionally measured κ_r into a site component κ_0, a possible source contribution κ_s and a general distance dependence function $\tilde{\kappa}(R_e)$, such that:

$$\kappa_r = \kappa_0 + \kappa_s + \tilde{\kappa}(R_e) \tag{1}$$

The classic approach of measuring κ_r on the acceleration FAS [11] is selected as the most pragmatic one for the purpose of the current study. As it requires the S wave spectra, a simple phase detection routine was employed to pick the adequate time windows automatically.

Due to the earthquake signal lengths ranging from only a few seconds to about 30 seconds, a windowed picking algorithm applied to a characteristic function derived from the waveform time series as in [19] would be too limited with respect to temporal precision. Further, that type of approach works best for P waves, whereas S wave arrivals are usually too obscured by the P wave coda. Thus, the method employed here relied on the evaluation of the maxima and minima of the detrended cumulative energy sums of the detrended trace windows containing the whole event waveforms. This requires the window to begin shortly before the P wave arrival and to end not too long after the surface wave coda. Exactly such time windows were produced by the SGM stations in Iceland, and the algorithm is robust enough to give a good S wave arrival estimate even in cases where the instrument triggered late and saved the record shortly after the P wave arrival.

Using the obtained time windows, κ_r was measured automatically by a relatively simple algorithm which adapts the used frequency band according to a selection of many frequency windows of which the optimal one is determined through a trade-off parameter. Windows with too low signal-to-noise ratio get rejected, and the trade-off parameter combines the root-mean-squared residuals between spectra and fitted lines (as a measure of linearity of the decaying log(FAS) versus linear frequency) with a frequency range term which penalizes narrower frequency ranges. This mostly results in excluding site resonance frequencies through the linearity constraint as a narrow-banded amplification would cause the selection to have higher deviance from a fitted line. A comparison to manual determinations showed that the differences in κ_r values are acceptably small, as the algorithm mostly avoids large site-dependent resonance frequencies due to its spectral linearity criterion. Due to the relatively low number of measurements and the considerable scatter in κ_r, a reliable distance dependence function $\tilde{\kappa}(R_e)$ could not be established. The analysis result as shown in *Fig. 2a* led to the decision of assuming an average value of 0.035 s as $\kappa_r = \kappa_0$ for the stations recording the SISZ earthquakes.

3.2 Data processing

To use the MCMC method in the Bayesian framework, data-based probability distributions had to be obtained with which synthetic data would be evaluated to yield model parameter distribution estimates. Here, spectral acceleration amplitudes from each event are gathered and their distributions for each frequency bin are required. Since the amplitudes are subject to several significant effects after the seismic waves leave their origin, they need to be corrected for these effects to yield a set of directly comparable data. These effects are geometric spreading, anelastic attenuation, near-surface attenuation and site amplification. Furthermore, the earthquake source itself not only determines the initial magnitude of the spectral amplitudes, but also their frequency-dependent shape. Therefore, source spectra were derived from S-wave spectra by applying measures which are described in the following paragraph, and an example is shown in *Fig. 3*.

First, mean and trend of the full acceleration time series of the two horizontal components were subtracted. The determined S wave time windows were then modified by a 5 % cosine taper and the geometric mean of their Fourier amplitude spectra was used from then on. The S wave window length was determined using the regional standard parameters for the ground motion model used, which gives a source duration in relation to the event's moment magnitude, and added to that a path duration of $T_P = 0.05[s/km]\ R_{epi}$.

The sensitivity to $\Delta\sigma_L$ is only significant above the patch corner frequency f_2, so the frequency bins below f_2 were excluded from the whole process. f_2 depends on the earthquake's subevent size and thereby on moment magnitude, global and local stress drop. This was further restricted for the larger events by setting a lower limit of 2.0 Hz to exclude near-source pulses, which are not included in this model.

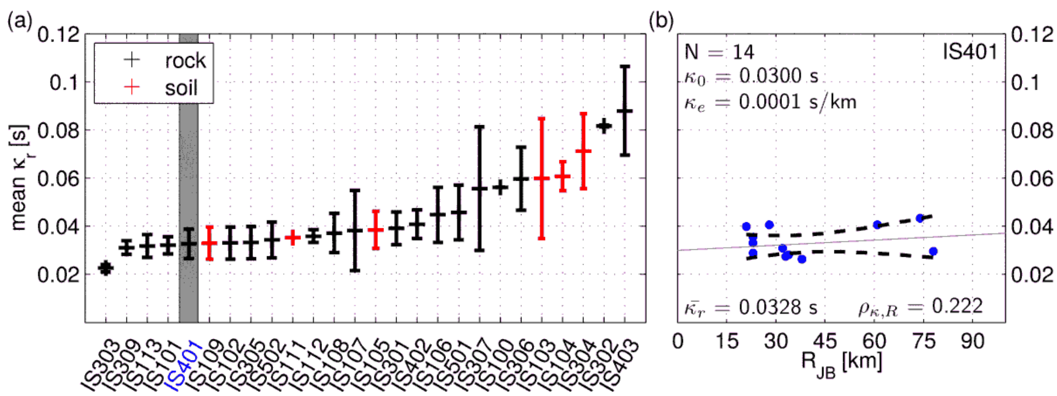

Fig. 2- Left: Mean κ_r values with one standard deviation for each station. Black and red colors indicate rock and stiff soil sites, respectively. Right: All Kappa measurements (geometric means of both horizontal components) for station IS401 as example for scatter and behavior over distance, with 95% confidence bounds for a fitted line. No stations showed a significant distance dependence of κ_r values.

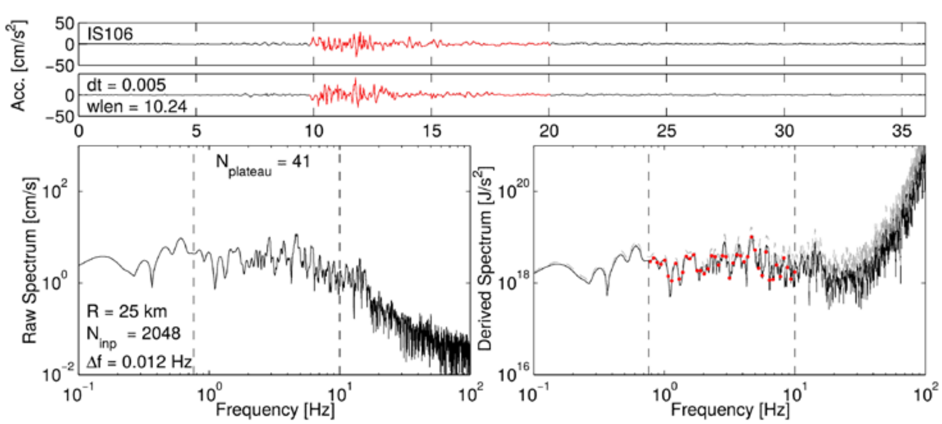

Fig. 3 – Raw horizontal acceleration waveforms (top) with selected shear wave phase in red. The geometric mean FAS of both components (bottom left) is shown with lower and upper analysis frequency limits indicated by dashed lines. The corrected spectrum (bottom right) represents the source acceleration spectrum, where black and gray curves are either without or with site amplification effect, respectively.

Amplitude decay due to geometric spreading, anelastic attenuation and scattering are corrected by a distance dependent geometric spreading function and a frequency and distance dependent attenuation function. The high frequency diminution is approximated by assuming one fixed κ_r for all stations and distances, because a more detailed parameterization could not be reliably established with the few existing measurements in the presence of large uncertainties. Here, the near-surface attenuation parameter was set to 0.035 s, as most stations fall close to that value. Site amplification is approximated using generic values representing rock and stiff soil, since detailed geotechnical information does not exist for the stations but site class estimations have been reported [15,16]. Site-specific amplification of lower to mid-range frequencies due to sediment layer reverberations causes distinct resonance peaks in some acceleration spectra, which are not accounted for in this analysis. Lastly, effects understood from theoretical seismology like radiation pattern, free surface effect and the distribution of energy to two components apply. Thus, a constant average scaling factor which is well established is applied to the spectra.

For the first method of inference using derived source FAS, data of the event from 1992-12-27 (id: 2) were excluded due to the low number of records. Further, traces without the full shear wave phase were excluded as well to yield the number of records given in *Table 1*. We have employed a second method of inference using a random effects model and inverting for seven model parameters simultaneously. In that procedure we include all seven events from *Table 1*, but excluded some records of the event from 2000-06-17 which were contaminated by energy from triggered earthquakes in the vicinity of the station [20]. Both methods used the same seismological model, but instead of using FAS value distributions the second method attempted to match response spectral accelerations. Therefore, the response of a single-degree-of-freedom (SDOF) harmonic oscillator with 5% damping was computed for the two horizontal components at 14 frequencies from 0.56 Hz to 23.7 Hz and subsequently the geometric mean of the peak spectral acceleration values at each frequency was taken.

3.3 Seismological model

Using the well-established stochastic modeling approach [21,22], the Fourier amplitude ground acceleration spectrum of an earthquake with seismic moment $M_{0,j}$ at receiver s_i and frequency f_k is:

$$Y(M_{0,j}, r_{ji}, s_i, f_k) = E(M_{0,j}, f_k) \cdot P(r_{ji}, f_k) \cdot G(s_i, f_k) \cdot I(f_k) \tag{2}$$

It consists of the earthquake source spectrum $E(M_{0,j}, f_k)$, the path effects $P(r_{ji}, f_k)$, the site-specific response function $G(s_i, f_k)$ and a transformation $I(f_k)$ for the type of motion (displacement, velocity, acceleration, SDOF harmonic oscillator response). The source spectrum is the displacement source spectrum $S(M_{0,j}, f_k)$ as defined by the Specific Barrier Model [2,3] multiplied by a constant scaling factor $C = \langle R_{\Theta\Phi}\rangle VF/(4\pi\rho\beta^3)$, where $\langle R_{\Theta\Phi}\rangle$ is the averaged radiation pattern (chosen as 0.55 from [23]), the partition factor into two horizontal components V=0.71, the free-surface effect F = 2, while ρ and β are density and shear wave velocity close to the source.

For the source spectrum, the Specific Barrier Model [1–7] is chosen due to its potential to better capture source complexity even as a point-source approximation through representing an earthquake source as agglomeration of small subevents. The resulting far-field spectrum has an analytic solution in that form which is characterized by two corner frequencies influenced by two different stress drop measures – the global stress drop $\Delta\sigma_G$, which represents the stress change across the whole fault including theoretically assumed barriers between subevents, and the local stress drop $\Delta\sigma_L$, which is the stress difference driving each subevent rupture and scales the level of radiated high-frequency waves.

The key equations of the SBM are given as follows [5–7,24]: The far-field source displacement spectrum $S(M_{0,j}, f_k)$ is expressed as

$$S(M_0, f) = \sqrt{\left(N + N(N-1)\left(\frac{\sin(\pi f T)}{\pi f}\right)^2\right)} D(M_{0_a}, f), \tag{3}$$

where the seismic moment M_0 is obtained from moment magnitude M_w [25]

$$M_0 = 10^{1.5(M_W - 6.07)}. \tag{4}$$

N is the number of subevents depending on the ratio between the two stress drop parameters

$$N = \left(\frac{\pi}{4}\right)^3 \left(\frac{\Delta\sigma_L}{\Delta\sigma_G}\right)^2. \tag{5}$$

The source duration T is proportional to the fault size, which is related to magnitude by

$$T = \frac{7\pi}{32\beta} M_0 (\Delta\sigma_G)^{\frac{1}{3}}. \tag{6}$$

The shear wave source displacement spectrum of a single subevent follows the ω-square model [26]

$$D\left(M_{0_a}, f\right) = \frac{M_{0_a}}{1+\left(\frac{f}{f_2}\right)^2}, \tag{7}$$

with M_{0a} being the seismic moment of a single subevent

$$M_{0_a} = \frac{M_0}{N}, \tag{8}$$

and the patch corner frequency f_2 according to Sato and Hirasawa [27]

$$f_2 = \frac{C_s \Delta\sigma_L \beta}{8\Delta\sigma_G} \left(\frac{16\Delta\sigma_G}{7M_0}\right)^{\frac{1}{3}}. \tag{9}$$

f_2 signifies the lower limit of significant influence of local stress drop $\Delta\sigma_L$ on the high frequency part of the source spectrum.

The path effects $P(r_{ji}, f_k)$ include geometrical spreading $Z(r_{ji})$ and anelastic attenuation $Q(r_{ji},f_k)$ as product $P(r_{ji}, f_k) = Z(r_{ji}) \cdot Q(r_{ji},f_k)$.The geometric spreading function uses two distance-dependent segments,

$$Z(r_{ij}) = \begin{cases} \dfrac{1}{r_{ji}} & , r_{ji} \le R_x \\ \dfrac{1}{\sqrt{R_x r_{ji}}} & , r_{ji} > R_x \end{cases}, \tag{10}$$

where R_x is the characteristic intermediate-field distance. The anelastic attenuation function contains the quality factor Q_0 and a frequency exponent α as attenuation parameters,

$$Q(r_{ji}, f_k) = \exp\left[\frac{-\pi r_{ji} f_k}{\beta Q_0 f_k^{\alpha}}\right]. \tag{11}$$

The distance r_{ji} is taken to physically approximate the distance to the closest significant seismogenic depth h at the epicenter such that $r_{ij}^2 = r_{epi}^2 + h^2$. Here, we assume h to be 3 km, representing the minimum depth to significant slip (subevents) on the basis of available static-slip distributions for the three largest earthquakes.

We defined the site response as $G(s_i, f_k) = A(s_i, f_k) \cdot K(s_i,f_k)$, the product of site amplification $A(s_i, f_k)$ due to shear wave velocity variation with depth in the upper ground layers and near-surface attenuation $K(s_i,f_k)$. The soil amplification curves were calculated through the quarter-wavelength approximation [28] assuming the sites can be categorized as either rock or stiff soil based on previous assessments [16] and choosing velocity profiles corresponding to NEHRP site classes B and BC [29], respectively. The near-surface attenuation in this study has the form $K(s_i,f_k) = \exp[-\pi\kappa_i f_k]$, where we chose to set κ_i to a constant κ_r of 0.035 s based on our independent measurement. For the second inference method using response spectral acceleration, random vibration theory in the context of the stochastic approach was used to simulate such data on the basis of the site spectrum. The approach as described in [22] is based on the extreme value theory for stationary random vibrations [30] and augmented by a vibration duration modification factor [31] to account for non-stationarity.

4. Statistical Modeling

4.1 Bayesian inference

Inference on the posterior distribution $\pi(\boldsymbol{\theta} \mid \boldsymbol{y})$ of model parameter vector $\boldsymbol{\theta}$ given data $\mathbf{y}$ requires knowledge about the sampling distribution $\pi(\boldsymbol{y} \mid \boldsymbol{\theta})$ also known as likelihood function and an assumption about the prior distribution $\pi(\boldsymbol{\theta})$,

$$\pi(\boldsymbol{\theta}|\boldsymbol{y}) \propto \pi(\boldsymbol{y}|\boldsymbol{\theta})\pi(\boldsymbol{\theta}). \tag{12}$$

The Markov chain Monte Carlo method is employed using a Metropolis step at each iteration. A Markov chain is a sequence of random variables $\theta^{(1)}, \theta^{(2)}, \ldots, \theta^{(t)}$, such that the current state $\theta^{(t)}$ only depends on the previous one $\theta^{(t-1)}$. The Metropolis algorithm produces the model parameter sequence by drawing a candidate value θ^* from a symmetric proposal distribution $q(\theta^* \mid \theta^{(t-1)})$. Here, a normal distribution with mean $\theta^{(t-1)}$ and a specified standard deviation is used, which should be adapted to the problem. The candidate value is either accepted or rejected based on the probability ratio

$$\alpha = \min\left\{1, \frac{\pi(\boldsymbol{\theta}^*|\boldsymbol{y})}{\pi(\boldsymbol{\theta}^{(t-1)}|\boldsymbol{y})}\right\}. \tag{13}$$

Upon rejection, the current proposed value is reset to the previous state. Given regularity, the Markov chain value distribution is expected to converge to the marginal posterior distribution $\pi(\boldsymbol{\theta} \mid \boldsymbol{y})$.

4.2 Method I

For the simpler first method in this study, there is just one free model parameter θ, the local stress drop $\Delta\sigma_L$. The derived source spectra using fixed seismological model parameters are used as data $\boldsymbol{y}$ for each event. Specifically, the spectral amplitudes A_k at each frequency f_k are assumed to follow a lognormal density,

$$\log(A_k) \sim Norm(\mu_k, \sigma_k) = \pi_j(\boldsymbol{y}|\theta). \tag{14}$$

The mean μ_k and variance σ_k values are calculated at each frequency f_k for each event j from all corresponding strong-motion records. For each randomly drawn stress drop in the Markov chains, a source spectral acceleration value is calculated at each frequency, its probability assessed according to eq. (12) and either accepted or rejected. The proposed $\Delta\sigma_L$ value is rejected if over 20% of the spectral amplitudes were rejected, otherwise it is accepted. That percentage was chosen by trial and error, since a higher threshold for rejection caused bad mixing and non-convergence whereas a lower threshold was too restrictive. A constant proposal standard deviation of 50 bar is used throughout. For prior knowledge about $\Delta\sigma_L$ it is assumed that the parameter must have a lower bound such that there is at least one subevent, which means according to eq. (5) that $\Delta\sigma_L$ is to be larger than 1.437 times $\Delta\sigma_G$.

4.3 Method II

We chose to infer several model parameters simultaneously for our second inversion approach to gain a better understanding of their relationships and uncertainties based on the ISMN dataset. We chose to invert based on pseudo-spectral acceleration (PSA) values instead of only Fourier amplitude values, this way stepping closer to engineering parameters of interest. As mean and standard deviation for PSA at each station and frequency for each event cannot be determined from the data due to being singular point measurements, unlike the derived source spectra in our first method, a simulation for every data point resulting in an equal number of misfit values is used to then argue that when using log(PSA) the misfit value distribution should be normal with unknown covariance. Thus, the likelihood function is based on the observation that the logarithm of the ratio between measured and simulated spectral acceleration (known as bias) at any given frequency follows a Gaussian distribution [2,32]. Defining a data covariance matrix which includes an inter-event variance σ^2 and an intra-event covariance term τ^2, we employ the random effects model [13,33]

$$\log y_{jik} = \mathcal{F}(M_j, r_{ji}, \boldsymbol{\theta}, f_k) + \eta_j + \epsilon_{jik}. \tag{15}$$

where y_{jik} is the PSA due to source j at location i and oscillator frequency f_k, $\boldsymbol{\theta}$ is a model parameter vector, η_j is the intra-event random effect and e_{jik} is the inter-event error.

In this study, the inferred model parameters are local stress drop $\Delta\sigma_L$, geometric attenuation crossover distance R_x, frequency dependent intrinsic and scattering attenuation function $Q(f) = Q_0 f^{\alpha}$, as well as two error terms σ^2 and τ^2 of the covariance matrix. We have defined their prior distributions to be uniform with reasonable lower and upper boundaries according to relevant literature [17,24,34,35]. To achieve efficient sampling and Markov chains with good mixing and convergence behavior, we devised an ad-hoc multi-stage adaptive tuning Metropolis algorithm, as the value ranges of the different parameters are quite different and bad mixing was the default when using a simpler MCMC implementation.

5. Results

Method I yielded approximately lognormal distributions (*Fig. 4*) for each event's local stress drop estimate. The values mostly range from 45 to 160 bar with mean values from 68 to 97 bar, except for the event from 2000-06-17, which has a significantly broader distribution at higher values from 65 to 270 bar (see *Table 2*). The average standard deviation is about 24 bar for most events and does not appear to depend on the number of recordings.

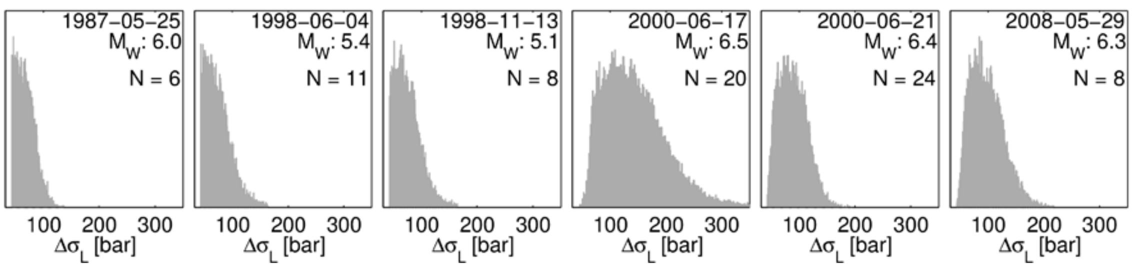

Fig. 4 – Histograms of $\Delta\sigma_L$ for all events. Event dates are indicated within the plots.

Table 2 – Posterior statistics of $\Delta\sigma_L$ distributions for all events.

				$\Delta\sigma_L$ [bar]					$\ln(\Delta\sigma_L)$	
Ev.ID	**Origin_time**	**M_W**	**N_{rec}**	**Mean**	**SD**	**2.5%**	**50%**	**97.5%**	**Mean**	**SD**
1	1987-05-25_11:31:56	6.0	6	67.6	16.5	44.2	65.6	104.6	4.18	0.24
3	1998-06-04_21:36:54	5.4	11	74.4	22.8	44.4	70.5	130.3	4.27	0.29
4	1998-11-13_10:38:34	5.1	8	75.5	22.4	44.6	72.0	128.6	4.28	0.29
5	2000-06-17_15:40:41	6.5	20	142.8	55.1	64.9	135.2	272.0	4.89	0.38
6	2000-06-21_00:51:48	6.4	24	88.3	24.7	49.7	86.2	140.3	4.44	0.28
7	2008-05-29_15:45:59	6.3	8	97.3	29.5	53.3	93.6	163.0	4.53	0.30

Method II shows a relatively narrow distribution around 100 bar for $\Delta\sigma_L$ with R_x being about 29 km, $Q(f) = 46.5 f^{0.89}$ and the total standard deviation in $\log_{10}$ units according to the covariance matrix is $\sigma_T = \sqrt{\sigma^2 + \tau^2} = 0.264$ (*Fig. 5*). The correlations between the parameters indicate that Q_0 and R_x are positively correlated, while α and Q_0 are negatively correlated, otherwise only some weaker correlations exist. The frequency-dependent bias and slope values with respect to distance and magnitude in *Fig. 6* show a good model fit for frequencies above 1 Hz up to 24 Hz and the bias is largest for the two lowest frequencies (0.56 to 0.75 Hz). The event-dependent random effect η_j appears to increase with magnitude.

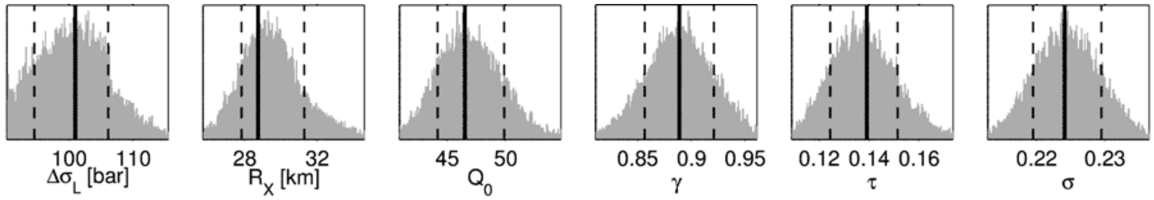

Fig. 5 – Histograms of the inferred parameter by Method II. The black line indicates the maximum likelihood estimate, while the dashed lines indicate the 16-84% credibility interval.

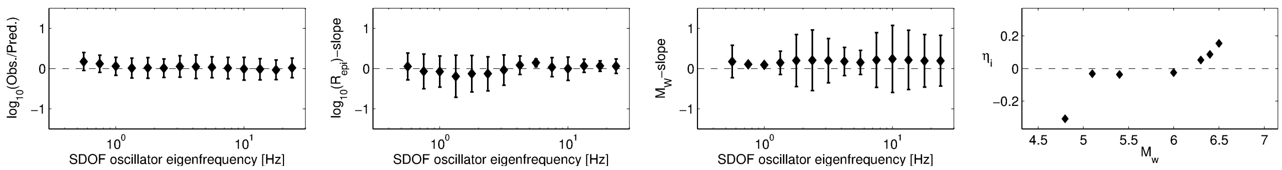

Fig. 6 – Model bias when using maximum likelihood estimates for the six parameters. Mean and one standard deviation at each frequency for bias (left), slope of bias with log(R_{epi}) (mid-left) and slope of bias with M_W (mid-right). The rightmost plot shows the distribution of inter-event residuals η_j versus magnitude.

6. Discussion

The stress drop estimates vary with each earthquake, but it could be argued that they remain similar within the this tectonic region. The estimates for the 17 June 2000 event diverge from the mean due to having included records containing energy of triggered events [20]. Allowing more model flexibility, a better estimate of the seismological parameters can be obtained, even though many details are still missing, such as exact site response and heterogeneous path effects. The scatter in the κ measurements seems somewhat arbitrary and a conservative assumption about its value for all stations seems justified in absence of better information.

The posterior stress drop distributions of Method I express the combined uncertainty resulting from site variations, path heterogeneities, radiation pattern and source complexity, which can be regarded as intra-event variability. The SBM has been calibrated already to various tectonic regions through optimization [24,36,37], but the parameters' uncertainties have not yet been established in that context. Through our approach in Method II we have shown an example for the uncertainty and relationship for some seismological parameters, but this would likely change depending on the prior assumptions and choice of free parameters. As this is a non-linear problem, we suggest that the use of such methods as Bayesian inference by MCMC algorithms can reveal important parameter relations and also irregular non-Gaussian distributions which would otherwise lead to faulty conclusions when treated through simple linear regressions. Additionally, there are still many sources of error, such as the lack of good site-specific response information and simplifying assumptions about the ground structure and the earthquake source itself.

7. Conclusions

The Icelandic strong-motion network in south Iceland continues to deliver useful information for the assessment of seismological parameters. The intra-event and inter-event variability of local stress drop $\Delta\sigma_L$ have been estimated for the SISZ, but the results need to be understood in the context of their parameterization. Different prior assumptions and fixed or free parameters should be used for further inversions to put these results into perspective. Then, due to the lack of strong-motion data in the Tjörnes Fracture Zone in North Iceland, the results for the SISZ presented here are, to the first approximation, assumed to apply there as well for the simulation of high-frequency earthquake strong-motion. The low frequencies (< 1 Hz) and the near-fault region can be explored further subsequently in the context of the SBM within the context of a kinematic and hybrid modeling approach.

8. Acknowledgements

This study was supported by the Icelandic Centre for Research (Grant of Excellence No. 141261-051/052/053), and partially by the Icelandic Catastrophe Insurance, and the Research Fund of the University of Iceland.

10. References

[1] Papageorgiou A S and Aki K (1983): A specific barrier model for the quantitative description of inhomogeneous faulting and the prediction of strong ground motion. I. Description of the model *Bull. Seismol. Soc. Am.* **73** 693–722

[2] Papageorgiou A S and Aki K (1983): A specific barrier model for the quantitative description of inhomogeneous faulting and the prediction of strong ground motion. Part II. Applications of the model *Bull. Seismol. Soc. Am.* **73** 953–78

[3] Papageorgiou A S (1988): On two characteristic frequencies of acceleration spectra: Patch corner frequency and f_{max} *Bull. Seismol. Soc. Am.* **78** 509–29

[4] Papageorgiou A S 2003 The Barrier Model and Strong Ground Motion *Pure Appl. Geophys.* **160** 603–34

[5] Halldorsson B and Papageorgiou A S (2012): Variations of the specific barrier model - Part I: Effect of subevent size distributions *Bull. Earthq. Eng.* **10** 1299–1319

[6] Halldorsson B and Papageorgiou A S (2012): Variations of the specific barrier model - Part II: Effect of isochron distributions *Bull. Earthq. Eng.* **10** 1321–1337

[7] Halldorsson B and Papageorgiou A S (2012): The effects of earthquake source complexities on far-field source spectra *15th World Conference on Earthquake Engineering (15WCEE)* (Lisbon, Portugal) p Paper no. 2543.

[8] Mavroeidis G P and Papageorgiou A S (2003): A mathematical representation of near-fault ground motions *Bull. Seismol. Soc. Am.* **93** 1099–1131

[9] Halldorsson B, Mavroeidis G P and Papageorgiou A S (2011): Near-Fault and Far-Field Strong Ground Motion Simulation for Earthquake Engineering Applications Using the Specific Barrier Model *J. Struct. Eng.* **137** 433–44

[10] Hanks T C 1982 f_{max} *Bull. Seismol. Soc. Am.* **72** 1867–79

[11] Anderson J G and Hough S E (1984): A model for the shape of the fourier amplitude spectrum of acceleration at high frequencies *Bull. Seismol. Soc. Am.* **74** 1969–93

[12] Ktenidou O-J, Cotton F, Abrahamson N A and Anderson J G (2014): Taxonomy of κ: A review of definitions and estimation approaches targeted to applications *Seismol. Res. Lett.* **85** 135–146

[13] Abrahamson N A and Youngs R R (1992): A stable algorithm for regression analyses using the random effects model *Bull. Seismol. Soc. Am.* **82** 505–10

[14] Sigbjörnsson R, Ólafsson S and Thórarinsson Ó (2004): Strong-motion recordings in Iceland *Proceedings of the 13th World Conference on Earthquake Engineering* (Vancouver, BC, Canada: Mira) p Paper no. 2370

[15] Þórarinsson Ó, Bessason B, Snæbjörnsson J T, Ólafsson S, Baldvinsson G I and Sigbjörnsson R (2002): The South Iceland earthquakes in 2000: Strong motion measurements *12th European Conference on Earthquake Engineering* (London, UK: Elsevier Science Ltd) p Paper no. 321

[16] Sigbjörnsson R and Ólafsson S (2004): On the South Iceland earthquakes in June 2000: strong-motion effects and damage *Boll. Geofis. Teor. Ed Appl.* **45** 131–52

[17] Halldorsson B, Ólafsson S and Sigbjörnsson R (2007): A Fast and Efficient Simulation of the Far-Fault and Near-Fault Earthquake Ground Motions Associated with the June 17 and 21, 2000, Earthquakes in South Iceland *J. Earthq. Eng.* **11** 343

[18] Toro G R, Abrahamson N A and Schneider J F (1997): Model of strong ground motions from earthquakes in central and eastern North America: best estimates and uncertainties *Seismol. Res. Lett.* **68** 41–57

[19] Baer M and Kradolfer U (1987): An automatic phase picker for local and teleseismic events *Bull. Seismol. Soc. Am.* **77** 1437–1445

[20] Pagli C, Pedersen R, Sigmundsson F and Feigl K L (2003): Triggered fault slip on June 17, 2000 on the Reykjanes Peninsula, SWIceland captured by radar interferometry *Geophys. Res. Lett.* **30** 1273

[21] Boore D M (1983): Stochastic simulation of high-frequency ground motions based on seismological models of the radiated spectra *Bull. Seismol. Soc. Am.* **73** 1865–94

[22] Boore D M (2003): Simulation of Ground Motion Using the Stochastic Method *Pure Appl. Geophys.* **160** 635–76

[23] Boore D M and Boatwright J (1984): Average body-wave radiation coefficients *Bull. Seismol. Soc. Am.* **74** 1615–1621

[24] Halldorsson B and Papageorgiou A S (2005): Calibration of the Specific Barrier Model to Earthquakes of Different Tectonic Regions *Bull. Seismol. Soc. Am.* **95** 1276–300

[25] Hanks T C and Kanamori H (1979): A moment magnitude scale *J. Geophys. Res. B* **84** 2348–50

[26] Aki K (1967 Scaling Law of Seismic Spectrum *J. Geophys. Res.* **72** 1217–31

[27] Sato T and Hirasawa T (1973): Body Wave Spectra from Propagating Shear Cracks *J. Phys. Earth* **21** 415–31

[28] Boore D M and Joyner W B (1997): Site amplifications for generic rock sites *Bull. Seismol. Soc. Am.* **87** 327–341

[29] Silva W J, Darragh R, Gregor N, Martin G, Abrahamson N A and Kircher C (2000): *Reassessment of Site Coefficients and Near-Fault Factors for Building Code Provisions* (Report to U.S. Geological Survey, National Earthquake Hazards Reduction Program. USGS Grant Award HQ-98-GR-01010)

[30] Cartwright De and Longuet-Higgins M S (1956): The statistical distribution of the maxima of a random function *Proceedings of the Royal Society of London A: Mathematical, Physical and Engineering Sciences* vol 237(The Royal Society)pp 212–232

[31] Liu L and Pezeshk S (1999): An improvement on the estimation of pseudoresponse spectral velocity using RVT method *Bull. Seismol. Soc. Am.* **89** 1384–1389

[32] Berrill J B (1975): A study of high-frequency strong ground motion from the San Fernando earthquake

[33] Brillinger D R and Preisler H K 1984 An exploratory analysis of the Joyner-Boore attenuation data *Bull. Seismol. Soc. Am.* **74** 1441–50

[34] Tryggvason A, Rögnvaldsson S T and Flóvenz O G (2002): Three-dimensional imaging of the P-and S-wave velocity structure and earthquake locations beneath Southwest Iceland *Geophys. J. Int.* **151** 848–866

[35] Bjarnason I T, Menke W, Flóvenz Ó G and Caress D (1993): Tomographic image of the mid-Atlantic plate boundary in southwestern Iceland *J. Geophys. Res. Solid Earth* **98** 6607–6622

[36] Papageorgiou A S and Aki K (1985): Scaling law of far-field spectra based on observed parameters of the specific barrier model *Pure Appl. Geophys.* **123** 353–74

[37] Foster K M, Halldorsson B, Green R A and Chapman M C (2012): Calibration of the Specific Barrier Model to the NGA Dataset *Seismol. Res. Lett.* **83** 566–74